

1 **Supplementary materials for**

2

3 **A millennium-long ‘Blue Ring’ chronology from the Spanish Pyrenees**
4 **reveals severe ephemeral summer cooling after volcanic eruptions**

5

6 **Running title: Blue Rings and volcanic eruptions**

7

8 Alma Piermattei¹, Alan Crivellaro^{1,2}, Paul J. Krusic^{1,3}, Jan Esper⁴, Petr Vitek⁵, Clive Oppenheimer¹,
9 Martin Felhofer⁶, Notburga Gierlinger⁶, Frederick Reinig⁴, Otmar Urban⁵, Anne Verstege⁷, Hannah
10 Lobo¹, Ulf Büntgen^{1,5,7,8,*}

11

12 ¹Department of Geography, University of Cambridge, United Kingdom. ²"Stefan cel Mare" University of Suceava, Romania. ³Department of Physical
13 Geography, Stockholm University, Sweden. ⁴Department of Geography, Johannes Gutenberg University, Mainz, Germany. ⁵Global Change Research
14 Institute of the Czech Academy of Sciences, Brno, Czech Republic. ⁶Department of Nanobiotechnology (DNBT), University of Natural Resources and
15 Life Sciences (BOKU), Vienna, Austria. ⁷Swiss Federal Research Institute, WSL, Birmensdorf, Switzerland. ⁸Department of Geography, Masaryk
16 University, Brno, Czech Republic. *Corresponding author: ulf.buentgen@geog.cam.ac.uk

17

18

19

20

21

22

23

24

25

26

27 Revised as an original research article to *Environmental Research Letters*, 19th September 2020

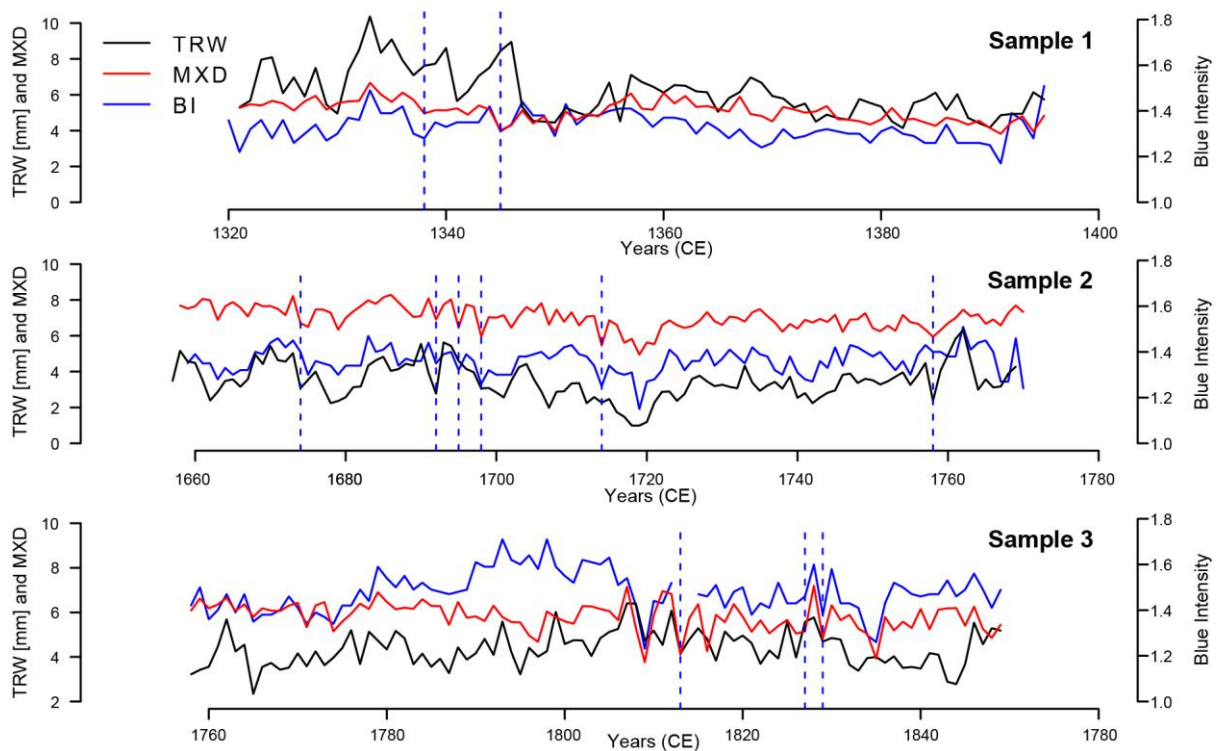
28 Raman imaging analyses were performed on a wood blocks with a Renishaw InVia spectrometer
29 (Renishaw, Wotton-under-Edge, UK) equipped with a confocal microscope (Leica, Wetzlar,
30 Germany). A point-to-point imaging mode was applied using a 20x magnification objective with
31 NA=0.40 was used (Leica, Wetzlar, Germany). The Raman scattering signal was collected by the
32 same objective and detected by Peltier-cooled CCD. A diode laser line at 785 nm was employed with
33 a 100 mW source power, 1 s exposure time, 1 accumulation at each point (50 mW power, 1s, and 3
34 accumulations for analysis of the extracted wood). The Raman signal was recorded in the 650–1750
35 cm^{-1} spectral range. Step-size of the piezo motorized scan stage XY movement was set to $6 \times 6 \mu\text{m}$.
36 The imaging acquisition was provided using the Wire 3.4 software interface (Renishaw, Wotton-
37 under-Edge, UK). The Raman image dataset processing was provided by the ImageLab software,
38 version 2.93 (Epina, Retz, Austria). Spikes (due to cosmic rays) were detected and removed using the
39 following parameters: spike half-width - 3; threshold - 1. Next, the spectra were smoothed out using
40 the Savitzky-Golay polynomial function, window: 7. Then, the baseline was corrected using the Eilers
41 algorithm using the following parameters: smoothness - 10000; asymmetry - 0.002; iterations - 7. The
42 images were created as intensity or ratio of intensities at particular wavenumber positions.

43 Microtome thin-sections were prepared for this purpose. The block was tightly clamped in a
44 rotary microtome (RM2235, Leica Biosystems Nussloch, Wetzlar, Germany) with an orientation
45 perpendicular to the main fibre axis. Disposable microtome blades (N35HR Blade 35° , Feather,
46 Osaka, Japan) were used to perform 10-20 μm thick transverse sections. During the cutting process,
47 only D_2O was used to avoid drying of the specimen. The thin sections were placed on a standard glass
48 slide with a drop of D_2O , covered with a glass coverslip (0.17 mm thick) and sealed with nail polish.
49 The BRS were marked on the bottom of the slide and measured immediately or kept frozen until the
50 analysis. Raman spectra were acquired with a Confocal Raman Microscope (alpha 300RA, WITec,
51 Ulm, Germany) equipped with a piezo motorized scan stage (x-y-z). The excitation light source was
52 a linear polarized (0°) coherent compass sapphire green laser at 532 nm (WITec, Ulm, Germany)
53 focused through a coverslip-corrected 100x oil objective (NA 1.4, Carl Zeiss, Jena, Germany). The

54 Raman scattering signal was collected by the same objective, delivered by an optic multifibre
55 (diameter = 50 μm) to the spectrometer (600 g mm^{-1} grating, UHTS 300 WITec) and finally recorded
56 by a CCD camera (Andor DU401ABV, Belfast, UK). The orientation of the sample with respect to
57 the laser polarization (the radial direction within the y-axis of the table) was kept constant during all
58 measurements. All Raman scans were taken with a lateral resolution of 0.3 μm by acquiring at every
59 pixel one spectrum with an integration time of 0.08 s and laser power of 35 mW. The control Four
60 (WITec) acquisition software was used to set experimental parameters for hyperspectral image
61 acquisition. Raman data analysis was performed with Project FOUR (WITec, Ulm, Germany)
62 software. The extracted spectra were analysed with Opus 7.5 software TM (Bruker, Rheinstetten,
63 Germany). Before the Raman images were generated based on integration of specific bands, a cosmic
64 ray removal filter was applied. Based on the integrated images, average spectra of distinct areas of
65 the samples (cell corner, cell wall, deposits) were obtained by drawing areas of interest or using an
66 intensity threshold.

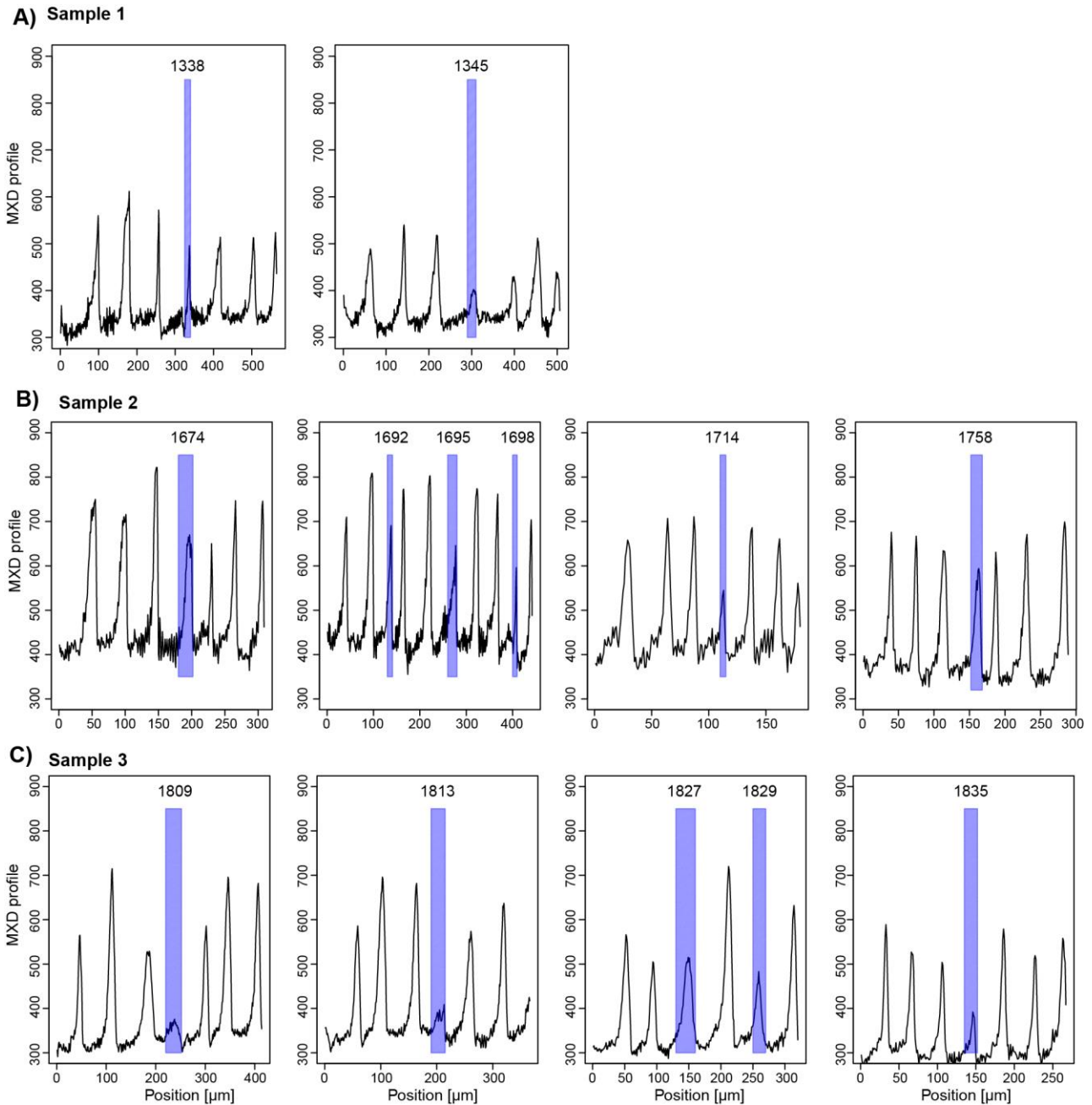
67

68 **Figures S1–S7 and Table S1**



69

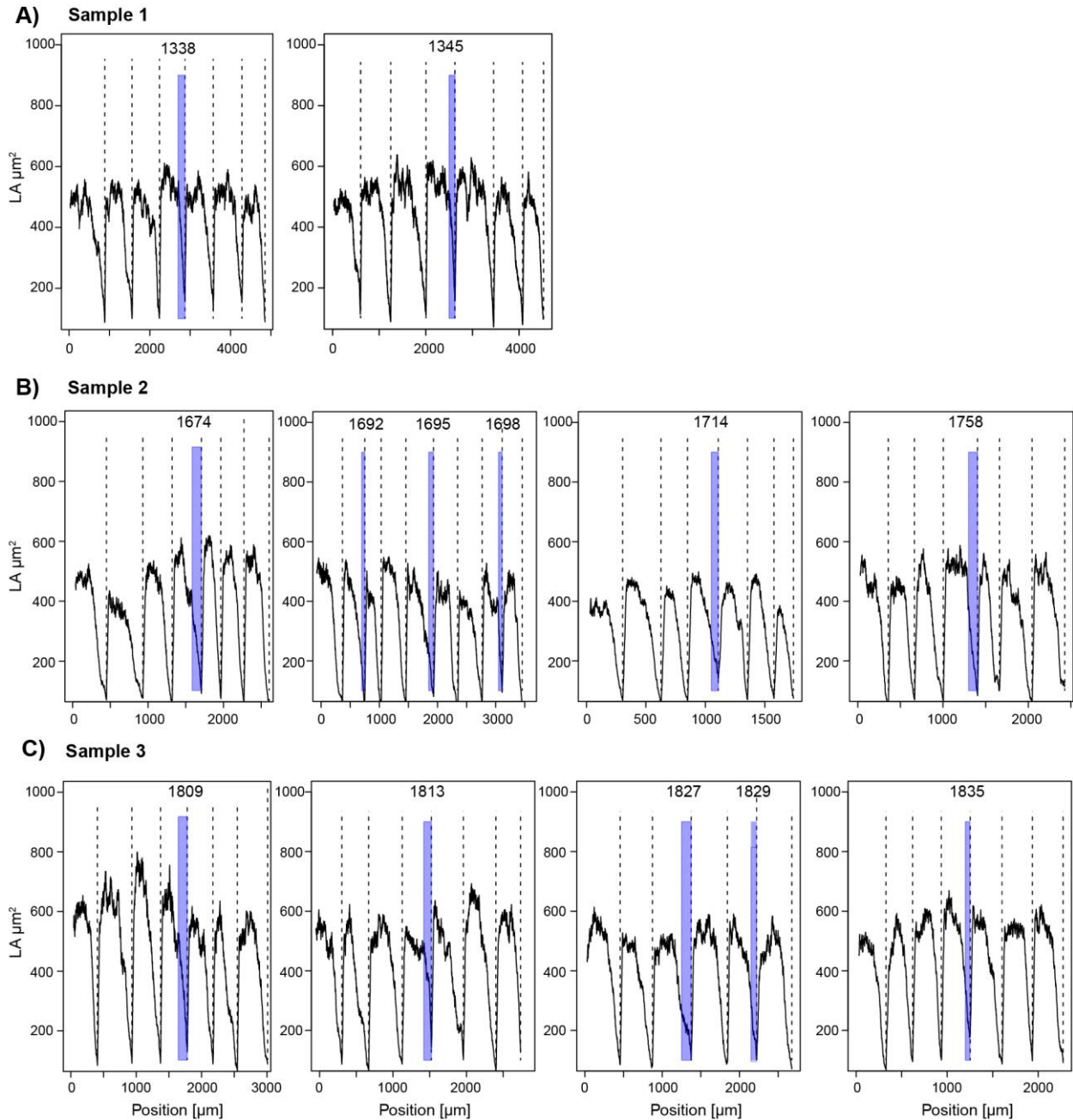
70 **Figure S1. Tree-ring width and maximum latewood density chronologies of three relict wood**
 71 **samples.** Trend of tree-ring width (TRW; mm; black line), maximum latewood density (MXD; g cm⁻³; red line), and Blue Intensity (BI; blue line) of the three historical samples spanning from 1320–
 72 1850 CE. The vertical dashed blue line shows the occurrence of BRs.
 73
 74



75
 76 **Figure S2. X-ray density profile of three relict wood samples. (A-C) X-Ray density profile (black**
 77 **line) of three years before and three years after BR occurrence from three relict samples spanning**

78 from 1320–1850 CE. The vertical blue rectangles show the latewood portion of the Blue Ring and
79 the date of each Blue Ring is written in each rectangle.

80

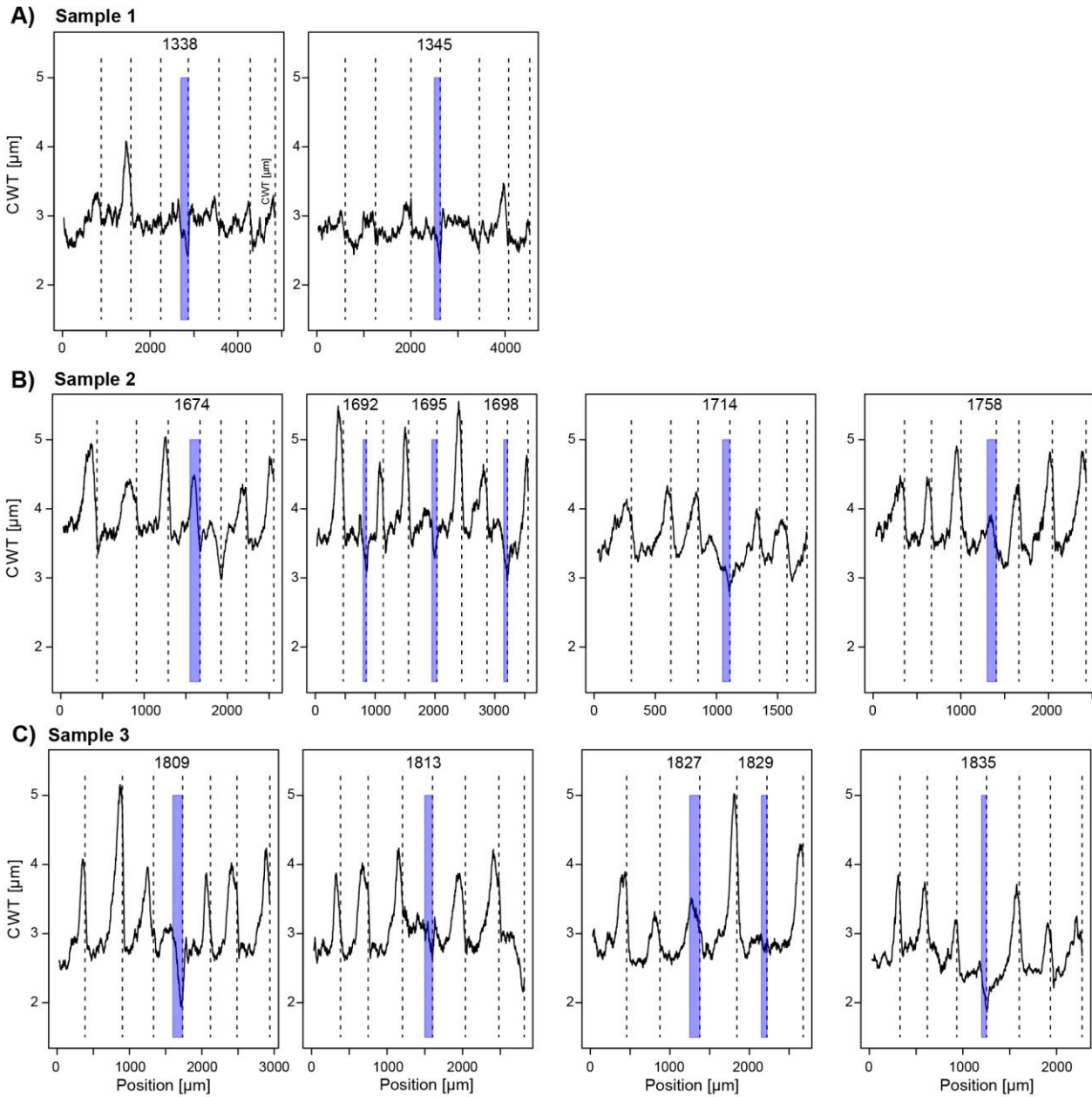


81

82 **Figure S3. Lumen area profile of three relict wood samples. (A-C)** Lumen area (LA) profile (black
83 line) of three years before and three years after a Blue Ring occurrence from the three relict samples
84 spanning from 1320–1850 CE. The vertical blue rectangles show the latewood portion of the Blue

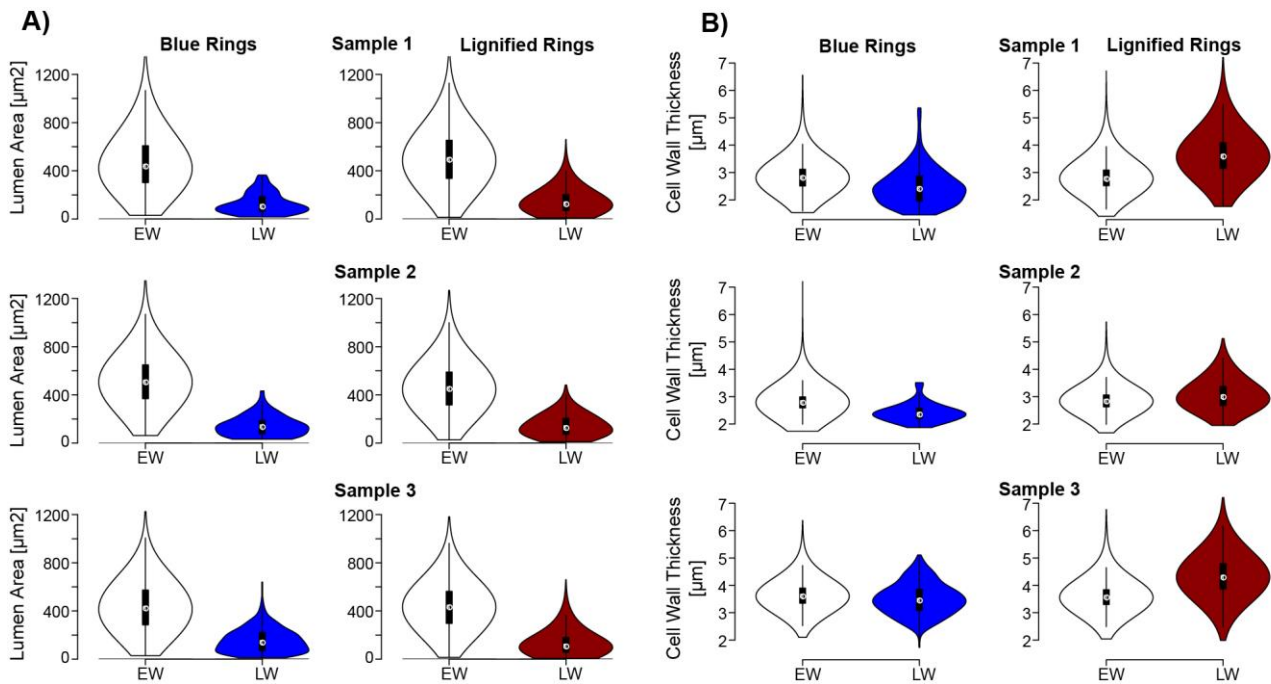
85 Ring and the date of each Blue Ring is written in each rectangle. The vertical dashed lines represent
86 the boundary of each ring.

87



88

89 **Figure S4. Cell Wall Thickness profile of three relict wood samples.** (A-C) Cell Wall Thickness
90 (CWT) profile (black line) of three years before and three years after a Blue Ring occurrence from
91 the three relict samples spanning from 1320–1850 CE. The vertical blue rectangles show the latewood
92 portion of the Blue Ring and the date of each Blue Ring is written in each rectangle. The vertical
93 dashed lines represent the boundary of each ring.



95

96

Figure S5. Lumen area and cell wall thickness of three relict wood samples. Violin plot of the

97

lumen area (LA) (A) and cell wall thickness (CWT) (B) of earlywood and latewood of BRs (no fully

98

lignified rings) and fully-lignified rings of the three relict samples spanning from 1320–1850 CE.

99

Only the latewood violin plots are in blue and in red for Blue Rings and for fully lignified rings,

100

respectively. The asterisk shows the statistical difference ($p < 0.001$) between BRs and fully lignified

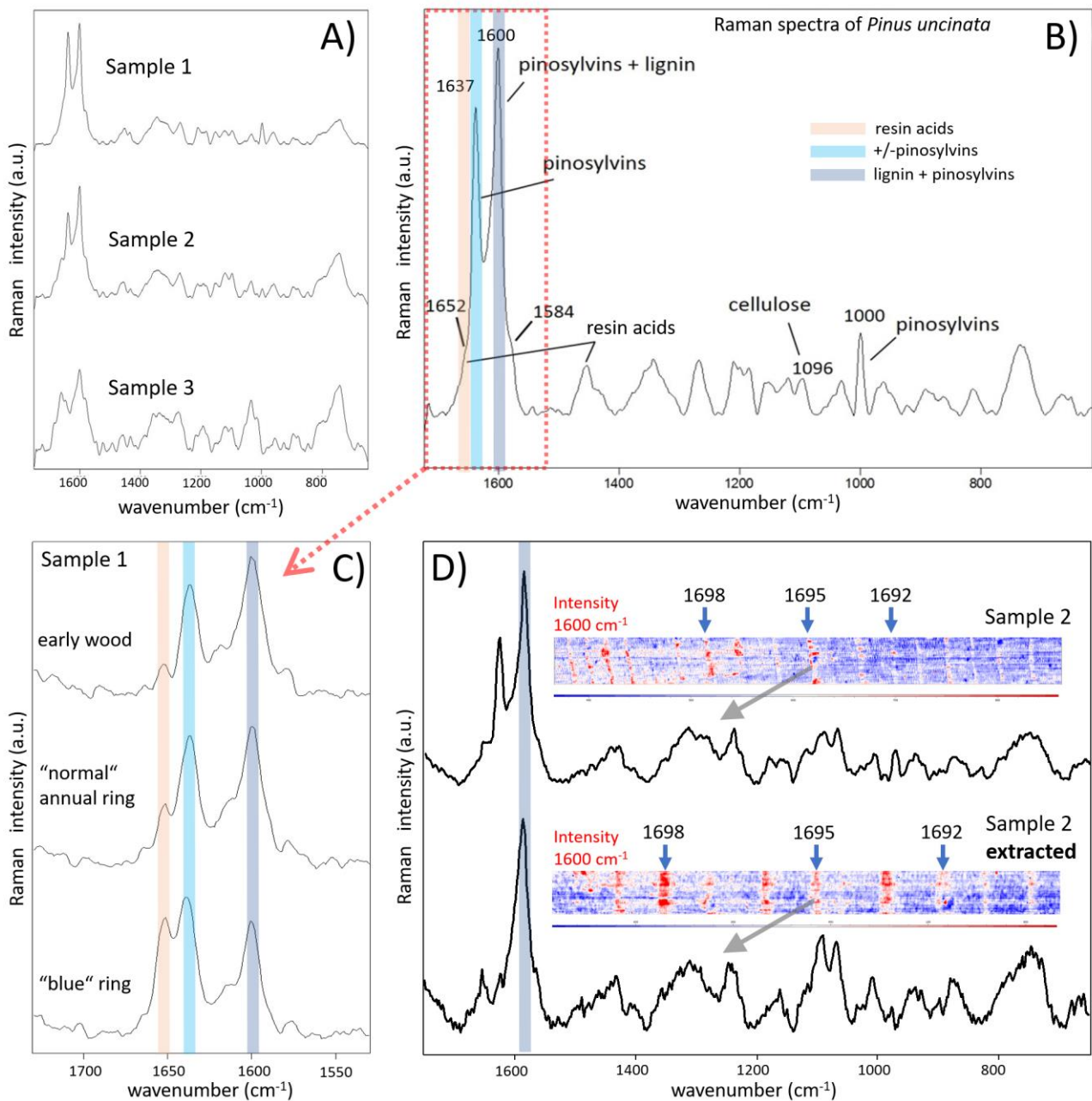
101

ring in the latewood portion. Latewood CWT of Blue Rings in the three samples is statistically

102

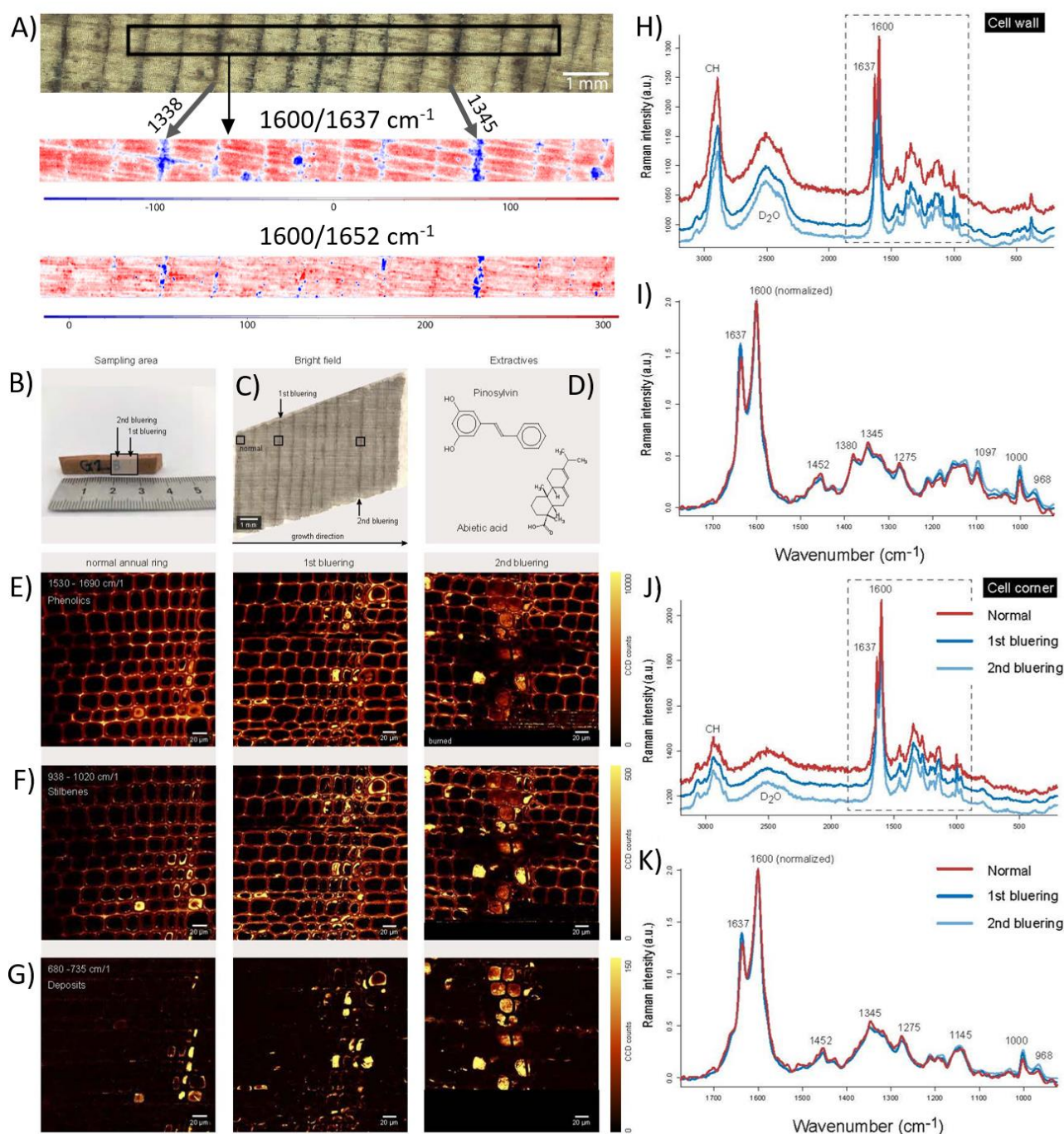
different to latewood CWT of fully lignified rings ($p < 0.001$).

103



104

105 **Figure S6. Raman spectroscopy and imaging of pine samples.** (A) Averaged Raman signal from
 106 the three measured samples. (B) Description of the most important bands of the typical Raman record
 107 from *Pinus uncinata*. (C) Magnified region of phenolics showing differences between "normal"
 108 annual ring, Blue Ring and early wood obtained on Sample 1. (D) Raman images (Sample 2)
 109 representing signal intensity at 1600 cm⁻¹, where lignin and pinosylvin features occur. The bottom
 110 image represents a dataset obtained on the sample after extraction of extractive phenolics, with lignin
 111 and cellulose dominating the spectra. Examples of spectra are averaged from multiple points from
 112 annual ring 1695. These Raman data were obtained using 785 nm excitation.



114

115 **Figure S7. In-situ Raman imaging of selected Blue Rings.** (A) Raman images obtained using 785
 116 nm excitation depicting distribution of 1600/1637 cm⁻¹ and 1600/1652 cm⁻¹ Raman band ratios.
 117 Enhanced signal at 1637 and 1652 cm⁻¹, represented by blue colour is due to pinosylvins and resin
 118 acids, respectively. (B) Pine wood block with the sampling area (rectangle). (C) Bright field image
 119 of a transverse microsection including two Blue Rings and the measurement areas. (D) Chemical
 120 formulae of the two extractive compounds. (E-G) Raman images at cellular level obtained using 532

121 nm excitation (normal, BRs in years 1338 and 1345) based on bands for **(E)** phenolic compounds
 122 (1530–1690 cm⁻¹), **(F)** stilbenes (938–1020 cm⁻¹) and **(G)** abietic acid (680–735 cm⁻¹). **(H-K)**
 123 Extracted spectra averaged from the zones of interest (from images **E-G**), including cell wall and cell
 124 corner; magnified spectral region is shown in **(K and I)**.

125

126 **Table S1. Blue Ring Inventory.** Each row represents the occurrence year of $\geq 20\%$ BRs and pBRs.
 127 For each BR and pBR the number of samples, TRW, MXD, and the reconstructed summer
 128 temperature (June–August) from 1186–2014 for Maximum Latewood Density expressed as
 129 temperature anomalies from the instrumental reference period 1961–1990 (Büntgen *et al* 2017) is
 130 listed in Wood Anatomy, and Dendro - Climate columns. The sum of the stratospheric aerosol optical
 131 depth (SAOD) for the North Hemisphere (NH) (Toohey and Sigl 2017), the name, location and
 132 estimated age of known volcanic eruption is listed in the volcanic forcing column. The value of SAOD
 133 represents the highest value in a window of ± 3 years from the occurrence of a BR or pBR. BR and
 134 pBR years that coincide with high SAOD values are marked in bold

Year	Wood Anatomy					Dendro - Climate				Volcanic Forcing		Estimated Eruption Date
	No. Sample	No. BRs	No. pBRs	% BRs ($\geq 20\%$)	%pBRs ($\geq 20\%$)	TRW (mm)	MXD (g/cm ³)	Temp. Anomalies	sum SAOD - NH (± 3 years)	Volcanic Eruption	Location	
1178	2	0	1	0	50	0.600	0.620	0.000	0.106 (1175)			
1180	2	0	1	0	50	0.530	0.570	0.000	3.018 (1182)			
1224	2	2	0	100	0	0.670	0.638	0.867	0.297 (1222)			
1233	2	1	0	50	0	0.750	0.618	-0.819	2.423 (1231)			
1258	5	4	1	80	20	0.810	0.506	-4.394	5.722 (1258)	Samalas	Indonesia	1257
1260	5	0	1	0	20	0.620	0.601	-1.791	1.284 (1260)			
1283	6	2	3	33	50	1.270	0.530	-2.924	0.041 (1283)			
1286	7	1	2	14	29	1.460	0.645	0.661	1.159 (1286)			
1288	7	3	4	43	57	0.970	0.490	-4.108	1.447 (1287)			
1290	8	4	0	50	0	0.810	0.562	-2.291	0.211 (1289)			
1298	8	4	0	50	0	0.830	0.615	-1.089	0.039 (1298)			
1305	8	0	2	0	25	0.980	0.591	-1.643	0.068 (1307)			
1331	11	0	3	0	27	1.020	0.664	0.906	1.131 (1329)			

1338	11	4	1	36	9	1.080	0.605	-1.138	0.386 (1341)			
1345	11	2	7	18	64	0.970	0.561	-2.425	1.193 (1345)			
1346	11	2	3	18	27	1.000	0.581	-1.833	1.487 (1346)			
1359	12	0	4	0	33	1.070	0.565	-2.033	0.039 (1359)			
1387	13	1	4	8	31	1.000	0.664	1.278	0.344 (1390)			
1394	13	3	1	23	8	0.870	0.641	0.062	0.052 (1393)			
1431	14	0	3	0	21	0.780	0.602	-1.564	0.039 (1431)			
1456	13	1	5	8	38	0.710	0.580	-1.690	1.092 (1454)			
1463	14	2	4	14	29	0.540	0.551	-2.338	1.048 (1460)			
1465	14	1	5	7	36	0.500	0.578	-1.576	0.260 (1463)			
1470	15	0	3	0	20	0.600	0.624	-0.028	0.451 (1470)			
1480	14	3	1	21	7	0.640	0.610	-0.554	1.455 (1477)			
1496	13	5	1	38	8	0.600	0.539	-3.748	0.039 (1496)			
1519	12	2	3	17	25	0.730	0.635	0.408	0.039 (1519)			
1544	12	4	2	33	17	0.550	0.564	-2.154	0.077 (1542)			
1574	12	4	1	33	8	0.640	0.587	-0.964	0.040 (1574)			
1576	12	3	3	25	25	0.600	0.553	-2.226	0.055 (1577)			
1587	12	5	1	42	8	0.600	0.528	-2.683	0.955 (1586)	Kelut	Indonesia	1586
1593	10	2	2	20	20	0.580	0.560	-1.881	0.061 (1591)			
1598	10	0	2	0	20	0.440	0.596	-0.708	0.899 (1596)			
1601	10	1	3	10	30	0.420	0.544	-2.435	2.090 (1601)	Huaynaputina	Peru	19.2.1600
1612	10	3	2	30	20	0.520	0.577	-1.287	0.039 (1612)			
1629	11	1	6	9	55	0.540	0.554	-2.351	0.039 (1629)			
1638	12	2	3	17	25	0.550	0.580	-1.720	0.424 (1637)			
1640	13	4	2	31	15	0.550	0.567	-2.021	1.938 (1641)			
1665	13	0	3	0	23	0.590	0.601	-0.938	0.968 (1668)			
1674	14	4	3	29	21	0.590	0.588	-1.172	0.509 (1674)			
1675	14	6	4	43	29	0.460	0.533	-3.616	0.251 (1675)			
1690	14	3	4	21	29	0.530	0.584	-0.806	0.039 (1690)			
1692	14	9	1	64	7	0.570	0.541	-2.448	0.276 (1694)			
1695	14	3	3	21	21	0.530	0.564	-1.634	1.287 (1695)			
1698	13	11	0	85	0	0.420	0.509	-3.894	1.516 (1696)			
1714	13	8	1	62	8	0.540	0.495	-4.006	0.039 (1714)			
1757	13	0	3	0	23	0.670	0.589	-1.147	0.378 (1756)			
1758	13	3	2	23	15	0.630	0.584	-1.969	0.163 (1757)			
1787	13	1	3	8	23	0.710	0.585	-1.920	4.282 (1784)			
1789	13	0	4	0	31	0.690	0.593	-1.619	0.683 (1787)			
1808	13	0	4	0	31	0.710	0.645	1.142	1.489 (1809)			

1809	13	4	5	31	38	0.620	0.570	-2.250	1.862 (1810)			
1813	13	4	1	31	8	0.600	0.591	-1.199	0.258 (1812)			
1816	13	0	4	0	31	0.550	0.562	-2.510	3.019 (1816)	Tambora	Indonesia	10.4.1815
1829	12	6	3	50	25	0.740	0.582	-1.421	1.155 (1831)			
1835	12	4	4	33	33	0.760	0.545	-2.916	0.998 (1836)	Cosigüina	Nicaragua	20.1.1835
1884	10	1	2	10	20	0.930	0.621	0.009	1.343 (1884)	Krakatau	Indonesia	26.8.1883
1885	10	2	1	20	10	0.980	0.645	1.140	0.689 (1885)			
1894	10	2	0	20	0	0.860	0.604	-0.713	0.786 (1891)			
1896	10	0	4	0	40	0.780	0.575	-1.831	0.048 (1896)			
1903	10	0	2	0	20	0.860	0.640	0.647	1.292 (1903)			
1905	9	0	2	0	22	0.960	0.627	0.277	0.621 (1904)			
1910	9	1	2	11	22	0.820	0.557	-2.357	1.239 (1912)			
1932	8	0	3	0	38	0.920	0.606	-0.409	0.199 (1929)			
1939	8	2	1	25	13	0.920	0.578	-1.750	0.057 (1939)			
1944	8	2	0	25	0	0.860	0.650	0.884	0.059 (1944)			
1974	6	2	0	33	0	0.850	0.605	-0.141	0.291 (1975)			
1993	5	1	0	20	0	0.900	0.664	2.048	1.237 (1992)			
1996	5	0	1	0	20	0.780	0.613	-0.035	0.226 (1994)			